Journal of Power Sources 217 (2012) 358–363

Contents lists available at SciVerse ScienceDirect

Journal of Power Sources

journal homepage: www.elsevier.com/locate/jpowsour

Mesoporous Co_3O_4 materials obtained from cobalt–citrate complex and their high capacitance behavior

Ru-Tao Wang [a], Ling-Bin Kong [a,*], Jun-Wei Lang [b], Xiao-Wei Wang [a], Shu-Qiong Fan [a], Yong-Chun Luo [a], Long Kang [a]

[a] State Key Laboratory of Gansu Advanced Non-ferrous Metal Materials, Lanzhou University of Technology, Lanzhou 730050, PR China
[b] State Key Laboratory of Solid Lubrication, Lanzhou Institute of Chemical Physics, Chinese Academy of Sciences, Lanzhou 730000, PR China

HIGHLIGHTS

- The mesoporous Co_3O_4 materials are synthesized from cobalt-citrate complex.
- The mesoporous Co_3O_4 materials have a large surface area of 129 $m^2\ g^{-1}$.
- The forming mechanism of mesoporous Co_3O_4 materials has been proposed.
- Mesoporous Co_3O_4 materials exhibit excellent electrochemical performance.

ARTICLE INFO

Article history:
Received 20 October 2011
Received in revised form
10 March 2012
Accepted 29 May 2012
Available online 13 June 2012

Keywords:
Electrochemical capacitors
Cobalt oxide
Cobalt–citrate complex
Cobalt hydroxide
Mesoporous

ABSTRACT

In this work, amorphous and mesoporous Co_3O_4 material is obtained from the calcination of loosely packed $Co_3O_4/Co(OH)_2$ nanosheets which are synthesized by the formation and disassociation of cobalt–citrate complex reaction. We propose that Co nanoparticles are completely oxidized to form the stable cobalt–citrate complex in the presence of sodium citrate and oxygen, and cobalt–citrate complex disassociates to $Co(OH)_2$ under alkaline conditions. The high surface area and mesoporous texture of granular Co_3O_4 materials are the consequence of the energetically favored topotactic transformation aspect in the solid-state oxidative reaction. Furthermore, mesoporous Co_3O_4 material exhibits excellent electrochemical capacitance prosperities, well retention to the discharging capacity in cycle lifetime, and a high specific capacitance of 427 F g^{-1}, indicating its potential application in electrochemical capacitors and further in energy and environmental applications.

1. Introduction

Cobalt oxide (Co_3O_4) represents an important class of inexpensive and environmentally benign materials with the potential applications in catalysts [1], magnetics [2], and high-performance electrochemical devices [3,4]. To design high-performance electrode materials in term of electrochemical activity, kinetic feature, retention to the discharging capacity in cycle lifetime, and understanding charge storage mechanism affect electrochemical performance is of great importance [5,6]. Recent studies prove that pseudocapacitors based on Co_3O_4 materials show much enhanced capacitance and greatly improved energy density compared with electric double-layer capacitors (EDLCs) [7–9]. However, there are still significant drawbacks of these Co_3O_4 pseudocapacitors, namely, the limited cyclical stability and poor rate capability of the Co_3O_4 electrode, which remain major challenges for use in practical batteries. These problems have long been partly attributed to low conductivity of metal oxides and phase transition (structural rearrangements) under the fast and reversible redox reaction at the surface of the electro-active materials in the charging/discharging electrochemical process [10–12]. The key to achieving high specific capacitance Co_3O_4 pseudocapacitors with long cycle life is to prepare nano-structured or micrometer-scale Co_3O_4 electrode materials with rational design of material morphology, size, and structure, which are critical to the electrochemical reactivity and lifetime based on reducing both the ionic and electronic path within the particles. Torsten Brezesinski et al. [10] proposed that mesostructured and nano-structured architectures for transition metal oxides facile both redox and intercalation pseudocapacitance

* Corresponding author. Tel.: +86 931 2976579; fax: +86 931 2976578.
E-mail address: konglb@lut.cn (L.-B. Kong).

0378-7753/$ – see front matter © 2012 Elsevier B.V. All rights reserved.
http://dx.doi.org/10.1016/j.jpowsour.2012.05.115

from alleviating the need of long-range diffusion of ions through the van der Waals gaps as well as amorphous structure can provide surface sites for redox pseudocapacitance. Recent advances in material preparation technologies enable electrode materials to be readily prepared with tunable particle size, shape and structure. For example, Zhu et al. [13] had synthesized Co_3O_4 materials with three different structures (one-dimensional needle-like nanorods, two-dimensional leaf-like nanosheets, and three-dimensional oval-shaped microparticles) by controlling the concentration of polyethylene glycol and water solution, which exhibit the promising capacitive properties. Mesoporous Co_3O_4 monolayer hollow-sphere array was fabricated by electrodepositing from aqueous solution containing cobalt precursor and exhibits a specific capacitances of 358 F g^{-1} at 2 A g^{-1} [14]. With the exposed crystal plane (112), Co_3O_4 nanomesh obtained from pyrolysis of the precursor of $(NH_4)_2Co_8(CO_3)_6(OH)\cdot 4H_2O$ and showed the high capacitances (155–198 F g^{-1}) and good rate capability [15].

Beyond that, there is a novel strategy basing on the rational design of complex reaction to prepare metal oxides with tunable particle size, shape and structure. Earlier examples of this strategy for the formation of cobalt oxides, such as CoO nanorods from Co–Oleate complex [16], Co_3O_4 nanotubes from (cysteinato-N,S) bis(ethylenediamine)cobalt(III) complex [17], hollow Co_3O_4 nanowire arrays from $[Co(NH_3)_6]_2^+$ [18], and CoO/Co_3O_4 composite nanocrystal from unknown complex [19], have been elegantly reported. It is anticipated that cobalt complex can be obtained by taking control of the rate of complex reaction and will serve as the precursor to fabricate meso-structural Co_3O_4 with the enhanced electrochemical performance.

Herein, we firstly report the preparation of amorphous and mesoporous Co_3O_4 nanomaterial which obtains from the pyrolysis of loosely packed $Co_3O_4/Co(OH)_2$ nanosheets based on the reaction of the formation and disassociation of cobalt–citrate complex. We propose that Co nanoparticles are completely oxidized to form the stable cobalt–citrate complex in the presence of sodium citrate and oxygen, and cobalt–citrate complex is disassociated to $Co(OH)_2$ under alkaline conditions. The high surface area and mesoporous texture of granular Co_3O_4 material might be the consequence of the energetically favored topotactic transformation aspect in the solid-state oxidative reaction. Furthermore, mesoporous Co_3O_4 material exhibits excellent electrochemical capacitance prosperities, well retention to the discharging capacity in cycle lifetime, and a high specific capacitance of 427 F g^{-1} that is obtained at a charge/discharge current density of 1.25 A g^{-1}, suggesting its potential applications in electrochemical capacitors and further in energy and environmental applications, such as lithium batteries, CO catalysis, and electrochemical evolution of oxygen.

2. Experimental

All solvents and chemicals are of reagent quality and are used without further purification. $Co(NO_3)_2\cdot 6H_2O$, sodium citrate (Na-Cit), $NaBH_4$, NaOH, and sodium lauryl sulfate (SDS) are obtained from Shanghai Chemical Reagent Co. All aqueous solutions were freshly prepared with deionized water. Scheme 1 shows the synthesis route of the mesoporous Co_3O_4 materials. In typical synthesis, 60 mg $Co(NO_3)_2\cdot 6H_2O$ and 180 mg Na-Cit were firstly dissolved in 30 ml distilled water under magnetic stirring. To this mixture, 5 ml of ice-cold $NaBH_4$ (0.1 M) was rapidly injected with stirring vigorously, generating a black solution. The whole solution was kept stirring vigorously for 2 h at room temperature to promote the oxidation of Co nanoparticles completely to form the stable cobalt–citrate species, as suggested by the color change of the solution from black to violet (Fig. S1). Then, 3 mg SDS and 60 mg NaOH dissolved in 5 ml distilled water were added to the mixture immediately. The reaction mixture was stirring vigorously for 5 min, and then left undisturbed at 30 °C for 36 h. Finally, a typical teal blue solid was shown, indicating the formation of $Co_3O_4/Co(OH)_2$ hybrid. The teal blue solid was collected and washed several times with ethanol and distilled water by centrifugation at 10,000 rpm, and finally dried at 80 °C for 4 h. By a subsequent thermal treatment at 250 °C for 3 h in air, the tea-blue $Co_3O_4/Co(OH)_2$ materials were changed into black Co_3O_4 powder. The more details of mechanism of Cobalt–Citrate Complex reaction were showed in supplementary material.

Transmission electron microscope (TEM) was carried out by using a JEOL JEM-2100 (Japan) operated at 200 kV. Morphology of the synthesized products was examined using a JEOL JSM-6701F (Japan) field emission scanning electron microscope (SEM). Wide-angle powder X-ray diffraction (XRD) patterns were obtained with a Rigaku D/Max-2400 (Japan) with Cu Kα radiation (40 kV,

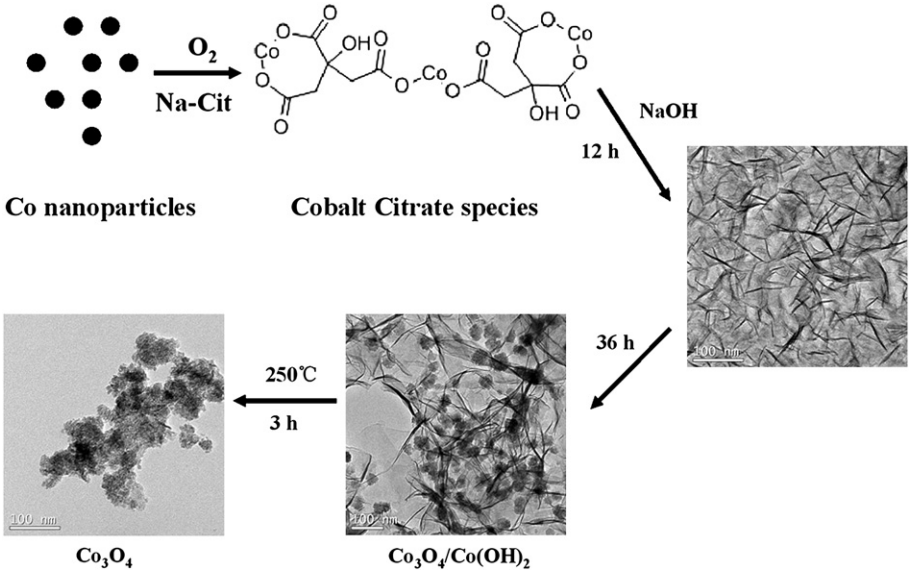

Scheme 1. Synthesis of meosporous Co_3O_4 materials from cobalt-citrate complex.

100 mA). Nitrogen adsorption-desorption data was obtained by using ASAP 2020 (Micromeritics, US).

The working electrodes were prepared according to the method in Ref. [20]. Co_3O_4 powder (80 wt%) was mixed with 7.5 wt% of acetylene black and 7.5 wt% of conducting graphite in an agate mortar until a homogeneous black powder was obtained. To this mixture, 5 wt% of poly(tetrafluoroethylene) was added with a few drops of ethanol. After briefly allowing the solvent to evaporate, the resulting paste was pressed at 10 MPa to nickel gauze with a nickel wire for an electric connection. The electrode assembly was dried for 10 h at 60 °C in air. Each electrode contained about 4 mg of electro-active material and had a geometric surface area of about 1 cm^2. Electrochemical measurements were carried out using an electrochemical working station (CHI660C, Shanghai, China) in a three-electrode at room temperature. 2 M aqueous solution of KOH was used as electrolyte. A platinum foam electrode (1 cm^2) and a saturated calomel electrode (SCE) served as the counter electrode and the reference electrode, respectively. Average specific capacitance values were calculated from the galvanostatic charge and discharge curves, using the following equation: $C = (I\triangle t)/(m\triangle V)$ (F g^{-1}), where I is constant charge or discharge current, $\triangle t$ is the time period for a full charge or discharge, m indicates the mass of the corresponding active electrode materials, and $\triangle V$ represents the voltage change after a full charge or discharge.

3. Results and discussion

X-ray diffraction (XRD) pattern shows that the as-prepared $Co_3O_4/Co(OH)_2$ nanostructures have the mixed Co_3O_4 spinel phase (JCPDS 42-1467) and layered α-$Co(OH)_2$ phase (JCPDS 46-0605) (Fig. 1). A plain view of loosely packed $Co_3O_4/Co(OH)_2$ nanostructures shows the irregular and curly morphology of the surface which exposes the edge planes and the random expansive open areas. Fig. 2a shows the cross section of the nanosheets is approximately 10 nm thick, and some small aggregates are loaded on the surface of the nanosheets. Transmission electron microscopy (TEM) images (Fig. 3a and b) indicate that the as-made $Co_3O_4/Co(OH)_2$ nanomaterial is composed of the nanosheets with curly layer morphology having the thickness about 10 nm and the monodisperse nanoparticles having a size dimension around 40 nm. These self-assembled nanosheets are firstly formed during the initial 12 h, and there are no any nanoparticles formed in this stage (Fig. S2). Upon further increasing the reacting time, the nanosheets become larger and the nanoparticles are formed. Note that SDS, as surfactant, should be present in the process of forming the loosely packed texture (Fig. S3).

By a subsequent thermal treatment in air at 250 °C for 3 h, the loosely packed $Co_3O_4/Co(OH)_2$ nanostructure is transformed into pure Co_3O_4 particles with mesoporous texture (Figs. 2b and 3c and d). The broad XRD peaks indicate low-crystalline nature of the cubic spinel Co_3O_4 materials (JCPDS 42-1467) (Fig. 1). The grain size of as-made Co_3O_4 material is ~8.9 nm as estimated with the Scherrer equation based on the (311) diffraction peak. The TEM images show that the as-made Co_3O_4 material is granule with irregular shape and mesoporous nature (Fig. 3c and d). The selected-area electron diffraction (SAED) and lattice spacing show well-defined rings, indicating their polycrystalline characteristics (Fig. 3d inset). All of the rings are contributed by the characteristic crystal planes of Co_3O_4, which can be ascribed to (311), (400), (511), and (440) from interior to exterior rings, consistent with the XRD results. Furthermore, the granular Co_3O_4 has a large surface area of 129 m^2 g^{-1} and the mesoporous structure with the pore size distribution centered at 3.7 nm and 4.7 nm, as measured by the Brunauer–Emmett–Teller (BET) measurements (Fig. 4).

To understand the reason why hybrid structure of $Co_3O_4/Co(OH)_2$ can be formed during the synthesis process, a formation mechanism is proposed and shown in Fig. 5. The first step is nucleation stage. Numerous $Co(OH)_2$ nucleation centers derive from disassociation of cobalt–citrate complex, which depend on the temperature and alkalinity. The second step is growing stage of nanosheet. Because of the anisotropy of $Co(OH)_2$ crystals, the

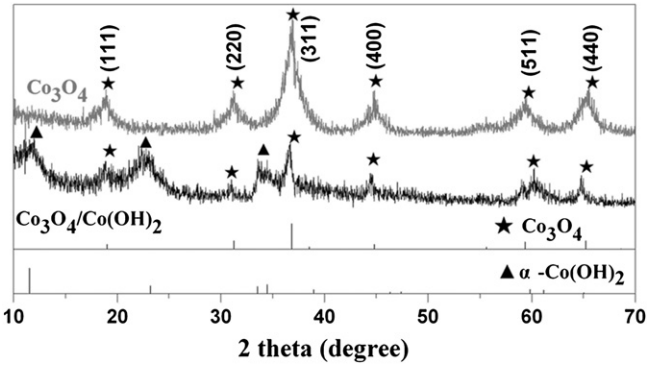

Fig. 1. XRD patterns of the $Co_3O_4/Co(OH)_2$ and Co_3O_4 nanomaterials.

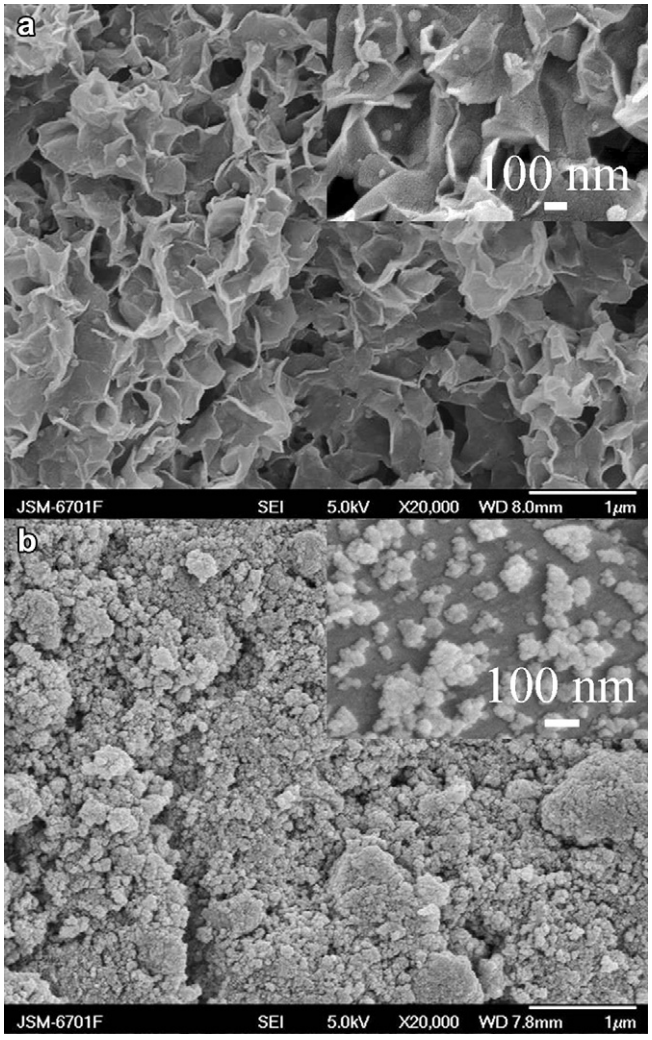

Fig. 2. Typical SEM images of (a) the loosely packed $Co_3O_4/Co(OH)_2$ nanostructures (magnified view of $Co_3O_4/Co(OH)_2$ nanostructures presented inset) and (b) the mesoporous Co_3O_4 materials (magnified view of Co_3O_4 materials presented inset).

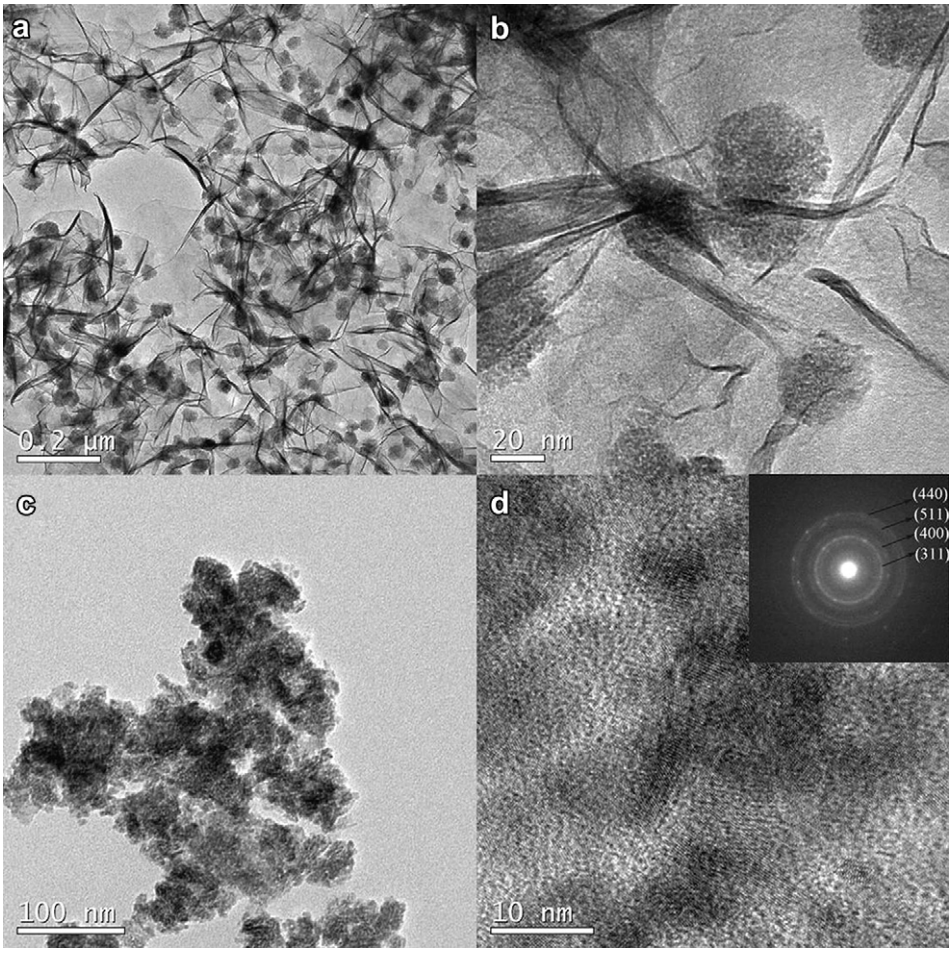

Fig. 3. (a) and (b) TEM characterization of the $Co_3O_4/Co(OH)_2$ nanomaterial with the curly layer morphology and the small nanoscale particles. (c) and (d) TEM and HRTEM characterization of the granular Co_3O_4 materials with mesoporous framework, (Inset image) the SAED pattern of the Co_3O_4 materials.

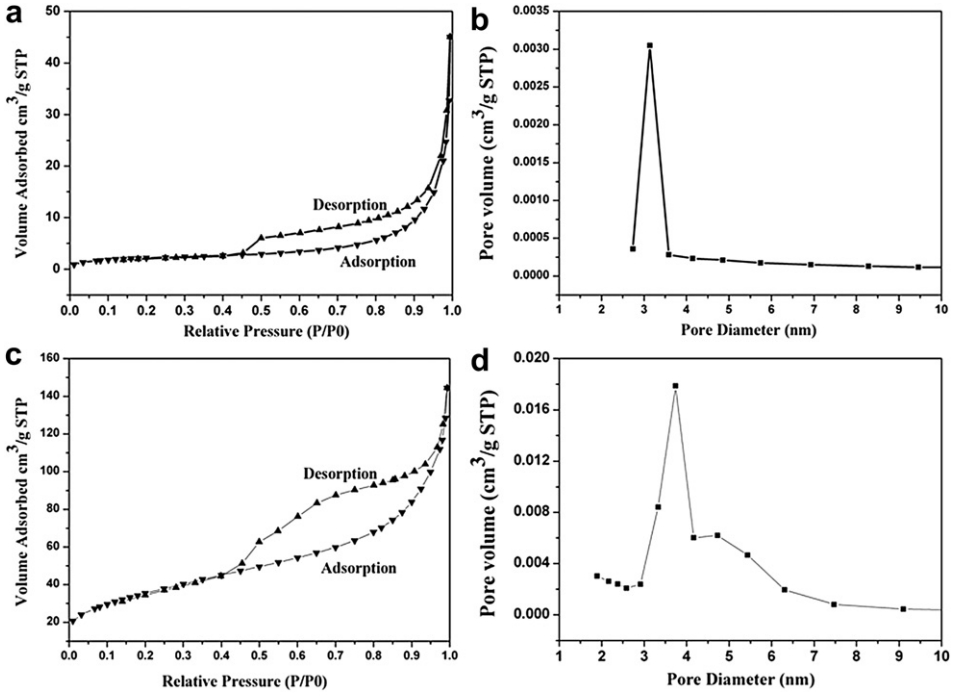

Fig. 4. BET measurements of the $Co_3O_4/Co(OH)_2$ sample (a), and the Co_3O_4 sample (c). The surface area of the $Co_3O_4/Co(OH)_2$ and Co_3O_4 is 8.14 $m^2\ g^{-1}$ and 129 $m^2\ g^{-1}$, respectively. The pore size distributions for the $Co_3O_4/Co(OH)_2$ and Co_3O_4 sample is shown in (b) and (d), respectively.

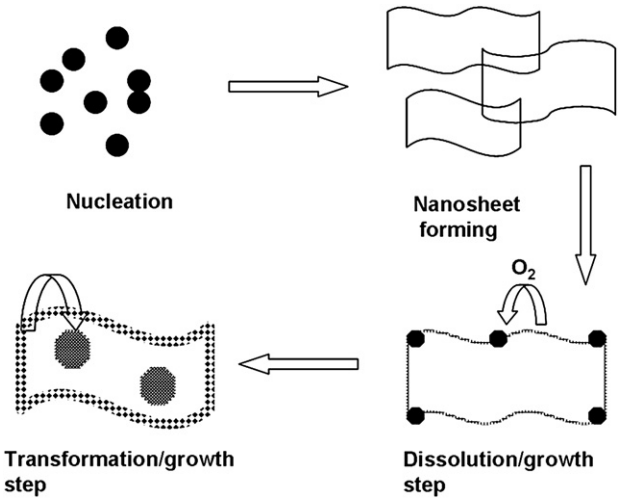

Fig. 5. Schematic formation mechanism of the as-prepared $Co_3O_4/Co(OH)_2$ sample.

growing point of each crystal is located at certain directions and cobalt–citrate complex slowly disassociates to provide precursors under the certain temperature, so nanosheets will be formed. More details of mechanism of Cobalt–Citrate Complex reaction were showed in Supplementary material. Herein, these $Co(OH)_2$ nanosheets do not agglomerate to the loose-packed nanoflower structure, indicating that the forming mechanism of $Co(OH)_2$ nanosheets is different from that of loose packed $Ni(OH)_2$ nanoflower in our previous studies [21]. The third step is dissolution and growth step. More specifically, nuclei of the CoOOH phase forms on the external part or on flake boundaries of the dissolved $Co(OH)_2$ nanosheet. The generation of transition-state CoOOH is because of that oxyhydroxides generally have smaller surface energies than oxides and are normally obtained by precipitation from aqueous solution [22]. The last step is transformation and growth step. The $Co(OH)_2$ continues to converted into transition-state CoOOH, and CoOOH can be reduced to Co_3O_4 at the low temperature due to reaction with oxygen and hydroxyl ions in the alkaline media, contrary to what is observed under other conditions where a temperature higher than 200 °C or the oxidant at lower temperature is required [23,24]. V. Pralong et al. suggest that the oxidation reaction is driven by solid-state amorphization including the dissolution of the $Co(OH)_2$ phase, the nucleating and growing process of the CoOOH and Co_3O_4 [24–26]. The solid state growth can induce strains in the nanosheets. Deriving from the unit cell mismatch among the hybrid phase, these strains are released to drive dislocation nucleation and motion, and then precipitate the nanosheets to form the highly porous particles with mesostructured texture. On the basis of the above studies, we propose that the hybrid structure of $Co_3O_4/Co(OH)_2$ nanomaterials originates from the solid-state reaction between the $Co(OH)_2$ nanosheets and the dissolved oxygen in the solution.

In the thermal treatment procedure, the obtained hybrid $Co(OH)_2$/CoOOH nanomaterial is calcined into spinel phase Co_3O_4 at 250 °C in air following the thermodynamically favorable solid-state oxidative reaction. The high surface area nature and porosity of granular Co_3O_4 might be the consequence of the energetically favored phase transformation aspect and strain relaxation in the solid-state oxidative reaction [27].

Electrochemical characterization and determination of the specific pseudocapacitance of the mesoporous Co_3O_4 material were investigated by cyclic voltammetry (CV) and charge/discharge test in a three-electrode beaker cell and a 2 M KOH electrolyte. It can be clearly observed the distinct redox peaks of a broad redox background in the CV curves (Fig. 6a). The redox

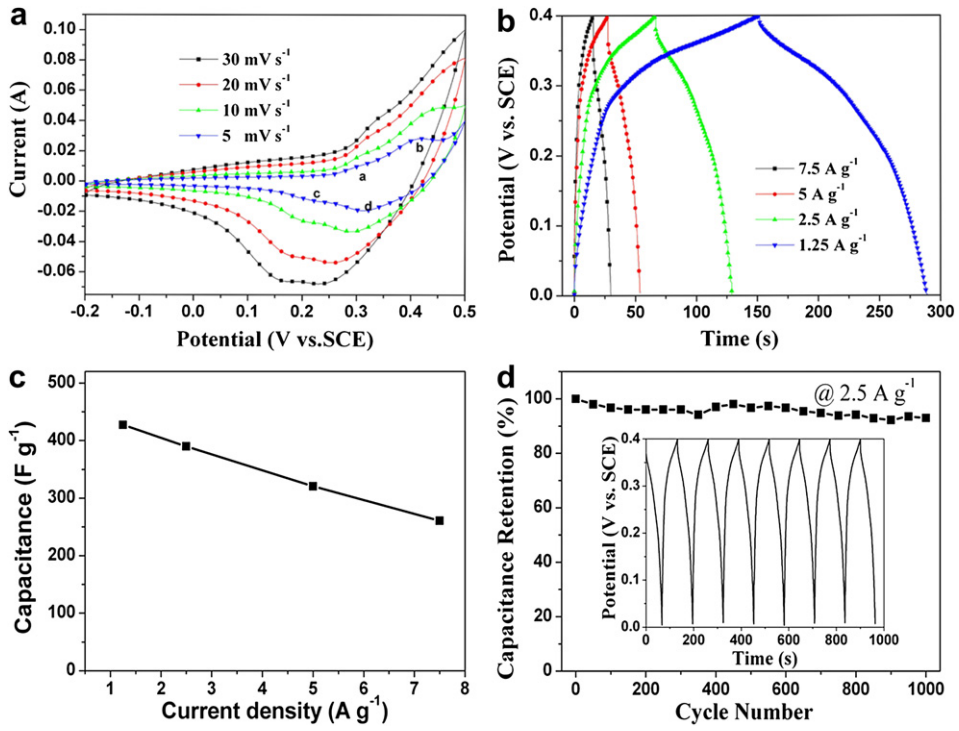

Fig. 6. Electrochemical characterization of mesoporous Co_3O_4 material: (a) CV curves of granular Co_3O_4 materials at various scan rates. (b) Galvanostatic charge and discharge curves of mesoporous Co_3O_4 material at various charge/discharge current densities. (c) Average specific capacitance of granular Co_3O_4 material at various charge/discharge current densities. (d) Average specific capacitance versus cycle number of mesoporous Co_3O_4 material at a galvanostatic charge/discharge current density 2.5 A g^{-1}, (Inner image) the galvanostatic charge/discharge curves of mesoporous Co_3O_4 material at a galvanostatic charge/discharge current density 2.5 A g^{-1}.

current peaks of Co_3O_4 electrode is represented by the following reactions [28].

Peak a and c (scan rate: 5 mV s^{-1}), CoOOH formation:

$$Co_3O_4 + OH^- + H_2O \leftrightarrow 3CoOOH + e^-$$

Peak b and d (scan rate: 5 mV s^{-1}), CoO_2 formation:

$$CoOOH + OH^- \leftrightarrow CoO_2 + H_2O + e^-$$

The average specific capacitance of the mesoporous Co_3O_4 material is calculated to be ~427 F g^{-1} at charge/discharge current density of 1.25 A g^{-1} and 261 F g^{-1} at a high charge/discharge current density of 7.5 A g^{-1}, ~61% of that at 1.25 A g^{-1} (Fig. 6b and c). The excellent charge/discharge stability of the mesoporous Co_3O_4 is demonstrated in Fig. 6d. After a cycle number of 1000 charge/discharge process at 2.5 A g^{-1}, the specific capacitance of the sample can be calculated from the discharge curves to be 365 F g^{-1}, indicting that as much as 93.5% of the initial capacitance (390 F g^{-1}) can be maintained for the mesoporous Co_3O_4 material. The enhanced specific capacitances and excellent cycle stability could be attributed to, first, amorphous structure for Co_3O_4 materials, providing many surface electro-active sites for redox pseudocapacitance; second, the advantageous high mesoporosity of nanoparticles, reducing the mass-transfer resistances, in favor of electrolyte penetration and ion diffusion; third, the highly specific surface area (BET surface area: 129 m^2 g^{-1}), enhancing the electrolyte/Co_3O_4 contact area and accommodating the transformation strains that originated from the volume change during the electrochemical reaction [10,29,30]. The little capacitance loss may be related to the microstructure changes of the mesoporous Co_3O_4 material in cycling test, which has been proved by TEM and XRD characterization and analysis (See Supplementary information for more details). These factors, we expect, should provide the improved specific capacitance and remarkable rate capability of the mesoporous Co_3O_4 materials for high-performance electrochemical pseudocapacitors.

4. Conclusions

In summary, we have developed a facile self-assembly method for preparing the mesoporous Co_3O_4 material using the common formation and disassociation of complex reaction and the solid-state oxidative reaction. The experimental conditions have been optimized to fabricate the Co_3O_4/$Co(OH)_2$ hybrid precursors which are composed of the nanoscale particles and the nanosheets with curly layer morphology. This method is important not only because it provides a facile method for the production of mesoporous Co_3O_4 material with the high specific area and the excellent electrochemical capacitance prosperities, but also because it exemplifies that the morphology and structure of the as-made materials could be tailored by the surfactant, temperature, and reaction time which also need more in-depth study in our further research. This synthesis protocol is expected to be applicable to other complex reactions for synthesizing metal hydroxides/oxides.

Acknowledgments

This work was supported by the National Natural Science Foundation of China (no. 21163010), the Key Project of Chinese Ministry of Education (no. 212183), and the Natural Science Funds for Distinguished Young Scholars of Gansu Province (no. 1111RJDA012).

Appendix A. Supplementary material

Supplementary material associated with this article can be found, in the online version, at http://dx.doi.org/10.1016/j.jpowsour.2012.05.115.

References

[1] W. Xie, Y. Li, Z.Q. Liu, H. Masatake, W.J. Shen, Nature 458 (2009) 746–749.
[2] E.L. Salabas, A. Rumplecker, F. Kleitz, F. Radu, F. Schüth, Nano Lett. 6 (2006) 2977–2981.
[3] X.L. Lou, D. Da, J.Y. Lee, J. Feng, L.A. Archer, Adv. Mater. 20 (2008) 258–262.
[4] G.X. Wang, H. Liu, J. Horvat, B. Wang, S.Z. Qiao, J. Park, H. Ahn, Chem. Eur. J. 16 (2010) 11020–11027.
[5] A.S. Aricò, P. Bruce, B. Scrosati, J.M. Tarascon, W.V. Schalkwijk, Nat. Mater. 4 (2005) 366–377.
[6] P. Simon, Y. Gogotsi, Nat. Mater. 7 (2008) 845–854.
[7] L. Cao, M. Lu, H.L. Li, J. Electrochem. Soc. 152 (2005) A871–A875.
[8] V. Srinivasan, J.W. Weidner, J. Power Sources 108 (2001) 15–20.
[9] J.W. Lang, X.B. Yan, Q.J. Xue, J. Power Sources 196 (2011) 7841–7846.
[10] T. Brezesinski, J. Wang, S.H. Tolbert, B. Dunn, Nat. Mater. 9 (2010) 146–151.
[11] G.H. Yu, L.B. Hu, M. Vosgueritchian, H.L. Wang, X. Xue, J.R. McDonough, X. Cui, Y. Cui, Z.N. Bao, Nano Lett. 11 (2011) 2905–2912.
[12] Q. Lu, M.W. Lattanzi, Y.P. Chen, X.M. Kou, W.F. Li, X. Fan, K.M. Unruh, J.G. Chen, J.Q. Xiao, Angew. Chem. Int. Ed. 50 (2011) 6847–6850.
[13] T. Zhu, J.S. Chen, X.W. Lou, J. Mater. Chem. 20 (2010) 7015–7020.
[14] X.H. Xia, J.P. Tu, X.L. Wang, C.D. Gu, X.B. Zhao, Chem. Commun. 47 (2011) 5786–5789.
[15] Y. Wang, H.J. Zhang, J. Wei, C.C. Wong, J.Y. Lin, A. Borgna, Energy Environ. Sci. 4 (2011) 1845–1854.
[16] K. An, N. Lee, J. Park, S.C. Kim, Y.S. Hwang, J.G. Park, J.Y. Kim, J.H. Park, M.J. Han, J. Yu, T. Hyeon, J. Am. Chem. Soc. 128 (2006) 9753–9760.
[17] X.Y. Shi, S.B. Han, R.J. Sanedrin, G. Galvez, D.G. Ho, B. Hermandz, F.M. Zhou, M. Selke, Nano Lett. 2 (2002) 289–293.
[18] X.H. Xia, J.P. Tu, Y.J. Mai, X.L. Wang, C.D. Gu, X.B. Zhao, J. Mater. Chem. 21 (2011) 9319–9325.
[19] L.P. Li, X.F. Sun, X.Q. Qiu, J.X. Xu, G.S. Li, Inorg. Chem. 47 (2008) 8839–8846.
[20] L.B. Kong, M. Liu, J.W. Lang, Y.C. Luo, L. Kang, J. Electrochem. Soc. 156 (2009) A1000–A1004.
[21] J.W. Lang, L.B. Kong, W.J. Wu, M. Liu, Y.C. Luo, L. Kang, J. Solid State Electrochem. 13 (2009) 333–340.
[22] A. Navrotsky, L. Mazeina, J. Majzlan, Science 319 (2008) 1635–1638.
[23] Z.S. Wu, W.C. Ren, L. Wen, L.B. Gao, J.P. Zhao, Z.P. Chen, G.M. Zhou, F. Li, H.M. Cheng, ACS Nano 4 (2010) 3187–3194.
[24] V. Pralong, A. Delahaye-Vidal, B. Beaudoin, J.B. Lercihe, J. Scoyer, J.M. Tarascon, J. Electrochem. Soc. 147 (2000) 2096–2103.
[25] V. Pralong, A. Delahaye-Vidal, B. Beaudoin, B. Gérand, J.M. Tarascon, J. Mater. Chem. 3 (1999) 955–960.
[26] V. Pralong, A. Delahaye-Vidal, B. Beaudoin, J.B. Lercihe, J.M. Tarascon, J. Electrochem. Soc. 147 (2000) 1306–1313.
[27] Y.G. Li, B. Tan, Y.Y. Wu, J. Am. Chem. Soc. 128 (2006) 14258–14259.
[28] B.Y. Kim, I.B. Shim, Z.O. Araci, S.S. Saavedra, O.L. Moti, N.R. Armstrong, R. Sahoo, D.N. Srivastava, J. Pyun, J. Am. Chem. Soc. 132 (2010) 3234–3235.
[29] T.Y. Wei, C.H. Chen, H.C. Chien, S.Y. Lu, C.C. Hu, Adv. Mater. 22 (2010) 347–351.
[30] J.P. Liu, J. Jiang, C.W. Cheng, H.X. Li, J.X. Zhang, H. Gong, H.J. Fan, Adv. Mater. 23 (2011) 2076–2081.